Volume 27
Number 30
14 August 2025
Pages 15805–16270

PCCP

Physical Chemistry Chemical Physics

rsc.li/pccp

25 YEARS ANNIVERSARY

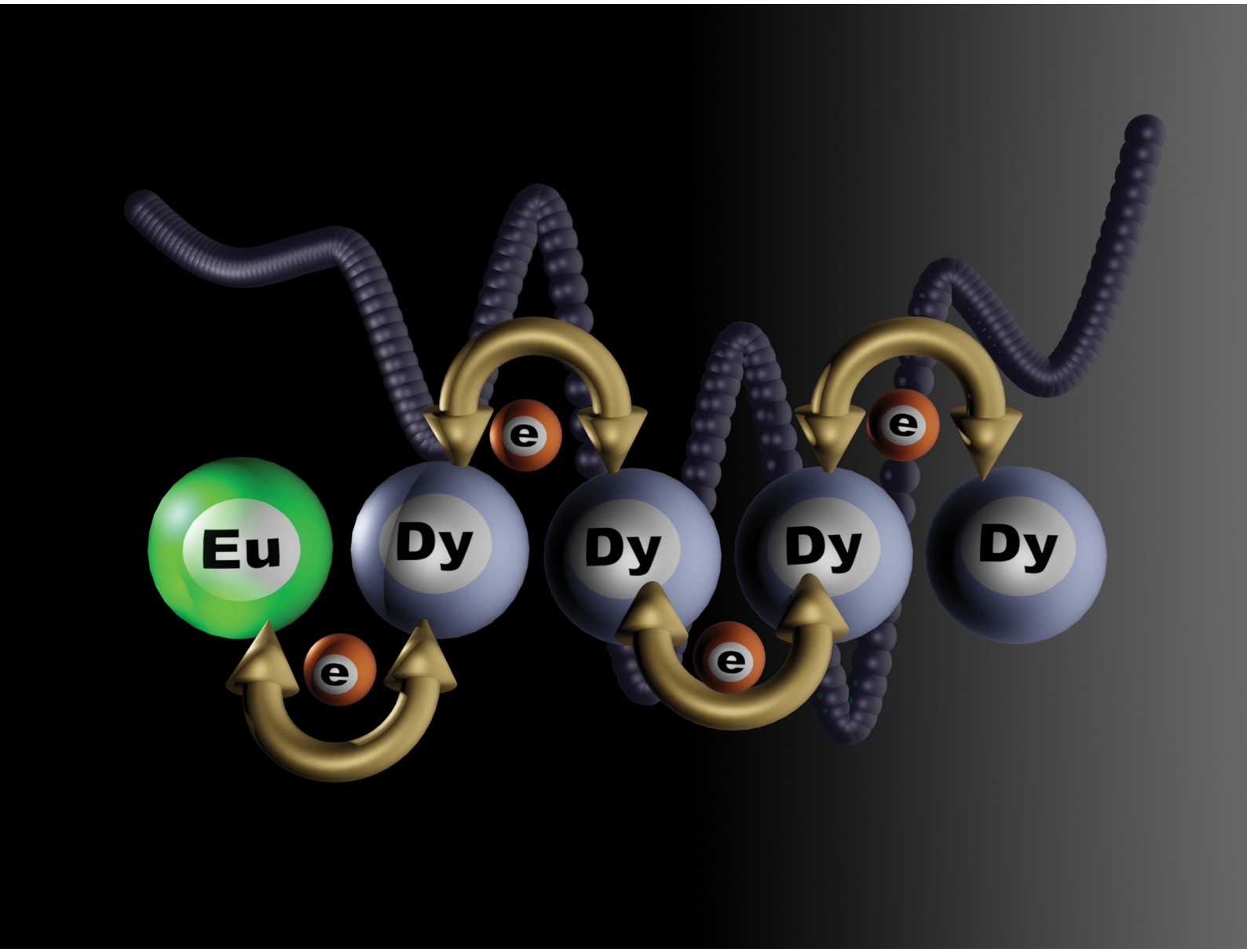

ISSN 1463-9076

ROYAL SOCIETY OF CHEMISTRY

PAPER

Kazuteru Shinozaki *et al.*

Visualization of trap distribution in $SrAl_2O_4:Eu^{2+},Dy^{3+}$ revealed by simulations of luminescence changes in charging and emission of persistent luminescence and thermoluminescence based on a random walk model

PCCP Owner Societies

PCCP

ROYAL SOCIETY OF CHEMISTRY

PAPER

View Article Online
View Journal | View Issue

Cite this: *Phys. Chem. Chem. Phys.*, 2025, **27**, 15850

Visualization of trap distribution in $SrAl_2O_4:Eu^{2+}$, Dy^{3+} revealed by simulations of luminescence changes in charging and emission of persistent luminescence and thermoluminescence based on a random walk model†

Ryusuke Koizumi, Ryoya Takahashi, Shigeki Yamada, Shingo Hattori and Kazuteru Shinozaki *

Received 31st March 2025,
Accepted 14th June 2025

DOI: 10.1039/d5cp01232e

rsc.li/pccp

A stochastic analysis of the change in persistent luminescence (PersL) of $Sr_{0.9}Al_2O_4:Eu_{0.01x}^{2+},Dy_{(0.1-0.01x)}^{3+}$ (SAOED$_x$, x = 2, 4, 5, 6, 8, and 10) based on a one-dimensional random walk model (1D RWM) is presented. In the RWM, the excited electron is treated as a particle and can hop stochastically between reservoirs aligned in a straight line. Simulations of changes in PersL and the charging process are performed to determine the hopping probabilities and the electron distributions in reservoirs. We predict potential energies of the electron reservoirs through simulations of the thermoluminescence (TL) spectra of SAOED$_x$ and present potential energy diagrams of the luminescence center and traps involved in PersL.

1. Introduction

Afterglow or persistent luminescence (PersL) has fascinated researchers involved in science and technology of light since the discovery of $SrAl_2O_4:Eu^{2+},Dy^{3+}$ (SAOED) exhibiting outstanding long PersL over one night.[1] Initially, PersL of SAOED has been employed for clock face as an alternative to radio-active materials or road signs without electrical power in the dark. Recently, it has been applied to photosensitizers and *in vivo* luminescent materials for photodynamic therapy,[2] optical imaging,[3] thermo-luminescence dosimetry,[4] and solar cells.[5] In addition to the application studies, many fundamental studies on PersL materials have been conducted to develop brighter phosphors with much longer lasting luminescence.[6–13] The photoluminescence (PL) of SAOED originates from the 5d–4f electronic transition of Eu^{2+} as a dopant, where the excited electron in the 5d orbital is usually relaxed to the 4f orbital with a lifetime of around 1 μs along with green luminescence.[14] For PersL, in contrast, the excited electron can be transferred to the host material by thermal or photoactivation and then be captured at trapping sites such as oxygen vacancies or defects, and thereafter the electron escaped from the trap by thermal activation returns to the 5d orbital of Eu^{3+} to reproduce the excited $^*Eu^{2+}$, resulting in emission of luminescence. The co-dopant Dy^{3+} plays the role of a better electron trap, which contributes to the longer PersL compared to oxygen vacancies or defects. The excited electron may be tightly captured by Dy^{3+} due to the electrostatic attraction, that is, Dy^{3+} might be reduced to Dy^{2+} by analogy to the result that Sm^{2+} and Ce^{4+} were detected during the investigation of the electron de-trapping process for an PersL material $YPO_4:Ce^{3+},Sm^{3+}$.[15]

Unlike PL, most PersL-decay features do not show a single-exponential curve. Therefore, the PersL decays have been frequently analysed using the double exponential equation,[14]

$$I(t) = I_0 + A_1 \exp(-t/\tau_1) + A_2 \exp(-t/\tau_2). \quad (1)$$

This equation consists of two exponential terms with the fast and slow decay times of τ_1 and τ_2, respectively, where τ_1 may be related to the de-trapping from the oxygen vacancy with a shallow trap depth and τ_2 may originate from the deep trap of Dy^{3+}. Occasionally, the PersL decay is analysed using the triple exponential function,

$$I(t) = I_0 + A_1 \exp(-t/\tau_1) + A_2 \exp(-t/\tau_2) + A_3 \exp(-t/\tau_3). \quad (2)$$

In this case, the additional component would be attributed to another trap involved in the PersL decay. Thus, it seems hard to find the electron-transfer mechanism satisfying the triple-exponential decay feature.

Some mechanisms for PersL proposed in previous studies are based on a local model composed of a single luminescent

Department of Material Science, Graduate School of Nanobiosystem Science, Yokohama City University, 22-2 Seto, Yokohama 236-0027, Japan.
E-mail: shino@yokohama-cu.ac.jp

† Electronic supplementary information (ESI) available: Experimental procedures and supplementary figures and tables. See DOI: https://doi.org/10.1039/d5cp01232e

centre and a single trap, where an excited electron is assumed to move back-and-forth between the luminescent centre and the trap in the PersL process.[16] In this model, the trap never captures two or more electrons, and the system of luminescence centres and traps is fully isolated and never interacts with others, that is, the electron cannot transfer to another trap in the adjacent system. In this situation, the observed PersL should always show a single-exponential decay curve, unless the electron transfer rates are slow compared with the time scale of PersL observation. On the other hand, a global model consisting of a luminescent centre, a trap, and the conduction band of host crystals has been applied to analyse the PersL decay.[17] The conduction band may be the pathway of electrons between the luminescent centre and the trap, and therefore the electrons involved in PersL would be distributed over the entire crystal in the PersL process. The electron transfer between the excited $*Eu^{2+}$ and the trap through the conduction band, based on the energy diagram with respect to the vacuum referred binding energy (VRBE) level,[18,19] has been taken into account for the PersL process. When electron de-trapping is caused by thermal activation, as per the Boltzmann distribution law, the ratio of the number of electrons in the luminescent centre and those in traps (oxygen vacancies and Dy^{3+}) is constant. Even when the excited electrons at the luminescence centre are consumed during the PersL emission, the immediate compensation of electrons from traps within the time scale of PersL observation guarantees that the ratio remains as the constant value. From this consideration, the PersL decay curve should follow a single exponential, even if multi-traps are incorporated in the global model. Therefore, it is better to consider that the electron transfer between the luminescence centre and the trap is slow or comparable to the time scale of PersL observation, when the PersL decay curve can be analysed with a double- or multi-exponential function. Previously, we showed that plural traps contribute to the complicated PersL-decay feature of β-$Zn_3(PO_4)_2$:Mn^{2+} through the stochastic analysis using a one-dimensional random walk model (1D RWM).[20] In the 1D RWM, the excited electron can randomly hop back-and-forth between adjacent traps and occasionally hop into the luminescent centre at the edge of the trap array to emit PersL.[20] The simulation for electron migration based on the RWM was found to be simple yet significantly effective to reproduce the multi-exponential PersL decays.

For SAOED, we can observe the luminescence enhancement during continuous excitation corresponding to the charge of PresL.[14] In this charging process, the luminescence intensity keeps increasing and eventually reaches the maximum value when the increase rate of excited electrons by photoexcitation is balanced with the depletion rate of electrons due to PL and PersL.[16] The excited electrons seem to be continuously transferred to/from the host material and accumulated in traps until filling up. When the photoirradiation ceased, we can observe PersL alone from SAOED. Both PersL and charging processes should be accounted for by the electron transfer between the excited state of $*Eu^{2+}$ and the trap state of (Eu^{3+}–$Trap^{-}$),[11] where the electrons can move between the potential surfaces of these states by overwhelming the activation state by thermal energy. Even when PersL disappeared due to the depletion of trapped electrons, luminescence can be recovered by other excited electrons squeezed out from deep traps by heating. The thermoluminescence (TL) spectrum, which is the luminescence observed at a variety of temperatures, provides information of trap depths in SAOED. A peak temperature in the TL spectrum is related to the trap depth, and the peak intensity is proportional to the number of escaped electrons from the trap.[21,22] Detailed analyses of the charging and PersL decay processes and the TL spectrum reveal the characteristics of dopants in SAOED and the mechanism of electron transfer between the luminescence centre and the trap involved in PersL.[23]

In this study, we show the effectiveness of the 1D RWM in simulating not only the non-exponential PersL decay curve of SAOED but also the charging process of PersL and TL. For the 1D RWM, we consider a train of multiple traps aligned in a straight line, where electrons can move back-and-forth between adjacent traps, and a luminescence centre is attached to the end of the trap line, where excitation of electrons and emission of luminescence take place. The simulation of the charging and PersL processes provides hopping probabilities among the luminescence centre and traps, corresponding to the electron transfer rates. Also, it provides evidence of electron population in traps, which helps to unveil the distribution of trap states in the SAOED crystal. In addition, the simulation of the TL spectrum provides the activation energy for each back-and-forth electron transfer process, which contributes to creating the energy diagram for traps involved in PersL for the SAOED crystal.

2. Simulation

2.1. A proposed mechanism of PersL emission

We propose a scheme for the PersL emission process based on the potential curves of Eu, *Eu, and trapping sites (Ts) in SAOED as shown in Fig. 1. The horizontal axis corresponds to a reaction coordinate along the electron transfer.[11] We denote that the excitation rate of Eu is k_0 and the relaxation rate of *Eu is k_e. The electron transfer rates between potential curves are k_m

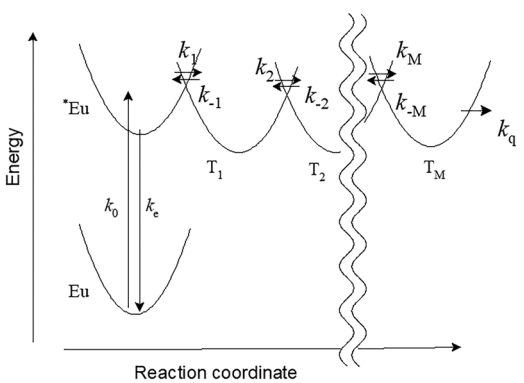

Fig. 1 A schematic energy diagram for Eu, *Eu, and T_m (m = 1, 2, …, M) for PersL of SAOED. k_m (m = ±1, ±2, …, ±M) are rate constants for electron transfer between potential wells.

($m = \pm1, \pm2, \ldots, \pm M$), and the capturing rate at deep trap or quenching rate is k_q. Although the tunnelling between potential curves might be necessary to consider the PersL emission mechanism, we do not treat the tunnelling explicitly in the RWM because all electrons are postulated to be particles. When focused on a single electron, a ground state configuration can be represented as G,

$$\mathrm{G}\text{: } (\mathrm{Eu})^{\mathrm{e}} - (^{*}\mathrm{Eu}) - (\mathrm{T}_1) - (\mathrm{T}_2) \cdots - (\mathrm{T}_M)$$

When *Eu is produced by photoexcitation, the electronic configuration can be represented as E_0,

$$\mathrm{E}_0\text{: } (\mathrm{Eu}) - (^{*}\mathrm{Eu})^{\mathrm{e}} - (\mathrm{T}_1) - (\mathrm{T}_2) \cdots - (\mathrm{T}_M)$$

The excited electron in the 5d orbital of *Eu can either relax to the 4f orbital to emit luminescence resulting in the G configuration or get trapped at closest trap T_1 which is represented as the E_1 configuration. The electron at T_1 (E_1) can move to the next trap T_2 (E_2) or return to the luminescence centre *Eu (E_1). The electron at T_2 can move to T_3 and so on,

$$\mathrm{E}_1\text{: } (\mathrm{Eu}) - (^{*}\mathrm{Eu}) - (\mathrm{T}_1)^{\mathrm{e}} - (\mathrm{T}_2) \cdots - (\mathrm{T}_M)$$

$$\mathrm{E}_2\text{: } (\mathrm{Eu}) - (^{*}\mathrm{Eu}) - (\mathrm{T}_1) - (\mathrm{T}_2)^{\mathrm{e}} \cdots - (\mathrm{T}_M)$$

$$\vdots$$

$$\mathrm{E}_M\text{: } (\mathrm{Eu}) - (^{*}\mathrm{Eu}) - (\mathrm{T}_1) - (\mathrm{T}_2) \cdots - (\mathrm{T}_M)^{\mathrm{e}}$$

Since there must be considerably many Eu ions in the bulk SAOED crystal, we should consider many sets of configurations $\{n_0\mathrm{E}_0, n_1\mathrm{E}_1, n_2\mathrm{E}_2, \ldots, n_M\mathrm{E}_M\}$ for the PersL process, where n_0, n_1, n_2, …, n_M are the numbers of respective excited configurations. We assume that this situation can be statistically equivalent to the following configuration with large numbers (n_0, n_1, n_2, …, n_M) of electrons in each trap:

$$(^{*}\mathrm{Eu})^{n_0\mathrm{e}} - (\mathrm{T}_1)^{n_1\mathrm{e}} - (\mathrm{T}_2)^{n_2\mathrm{e}} \cdots - (\mathrm{T}_M)^{n_M\mathrm{e}}$$

When n_0 is decreased by luminescence emission, it will be compensated by the electron transfer from T_1 to *Eu, which contributes to the elongation of the luminescence lifetime resulting in PersL. Since the emission intensity is proportional to the product of n_0 and k_e, the simulation of PersL decay is equivalent to the determination of n_0k_e as a function of t. The simulation will provide not only n_0 and k_e but also the other rate constants $k_{\pm m}$ and the number of electrons (n_1, n_2, …, n_M) in each trap. For the charging process, since $n_m = 0$ ($m = 0, 1, 2, \ldots, M$) at the beginning, the photoexcitation contributes to an increase in n_0 alone. After that, while n_0 gradually decreases by the electron transfer to T_1 and the relaxation to Eu, the continuous photoexcitation from Eu and the backward electron transfer from T_1 contribute to an increase in n_0. Thus, n_0 initially increases and eventually will reach the maximum value when the increase and decrease rates of n_0 are balanced. This charging process should also be simulated from n_0k_e as a function of t using the rate constants determined by the PersL simulation. Since the electron transfer rate k_m corresponds to the de-trapping rate of electrons from the potential well, it would strongly depend on temperature. Therefore, for simulations of the TL spectrum, the temperature dependence in the rate constant $k_{\pm m}$ can be incorporated as

$$k_{\pm m} = k_{0,\pm m} \exp(-\Delta E_{\pm m}/k_{\mathrm{B}}T), \quad (3)$$

where $k_{0,\pm m}$ ($m = 1, 2, \ldots, M$) are pre-exponential factors, $\Delta E_{\pm m}$ is trap depth or activation energy for each electron transfer process, k_B is Boltzmann's constant, and T is the absolute temperature. The simulation of the TL spectrum is equivalent to the prediction of n_0 as a function of T and contributes to the determination of the activation energies for electron transfer ($\Delta E_{\pm m}$).

2.2. A 1D random walk model (1D RWM) for the PersL

Based on the mechanism described above, we stochastically simulate the change in luminescence of the charging process, the non-exponential decay of PersL, and the TL spectrum using the 1D RWM as displayed in Fig. 2. The rectangle reservoirs being able to store electrons are aligned in a straight line, where each reservoir represents Eu, *Eu, or Ts. Eu is fixed at the left end, and *Eu is next to it. An array of Ts is set next to *Eu. We treat Dy^{3+} and other traps (oxygen vacancies or defects) as the same T_m. We assume that the electrons can move forward and backward between the very next reservoirs with certain probabilities, respectively, or can remain at the same reservoir. We introduce an electron-extinction path from T_M to represent the dropping in deep traps or the quenching. In this model, we introduce a probability p_m for each hopping between reservoirs instead of the electron-transfer rate constant k_m. Since the electron-transfer rate (k_m) to overwhelm the activation barrier (ΔE_m) is represented as $k_m = k_{m,0}\exp(-\Delta E_m/k_{\mathrm{B}}T)$, we can describe the hopping probability as

$$p_m = k_m/k_{m,0} = \exp(-\Delta E_m/k_{\mathrm{B}}T). \quad (4)$$

For example, the electron at Eu can move to *Eu with a probability p_0 ($0 \le p_0 \le 1$) upon excitation. For the electron at *Eu, the probabilities of moving to Eu and T_1 are p_e ($0 \le p_e \le 1$) and p_1 ($0 \le p_1 \le 1$), respectively, and probability of remaining at *Eu is $1 - p_e - p_1$.

We define the number of electrons at reservoirs as N_0 at *Eu and N_m at T_m ($m = 1, 2, \ldots, M$). For the random walk of electrons in the charging process, we initially prepare Eu with N electrons and the empty *Eu and Ts, that is, $N_m^0 = 0$ ($m = 0, 1, 2, \ldots, M$). After the first step, Np_0 electrons move to *Eu from Eu, but $N(1 - p_0)$ electrons remain in Eu, that is, $N_0^{\,1} = Np_0$ and $N_m^{\,1} = 0$ ($m = 1, 2, \ldots, M$). After the second step, we can find

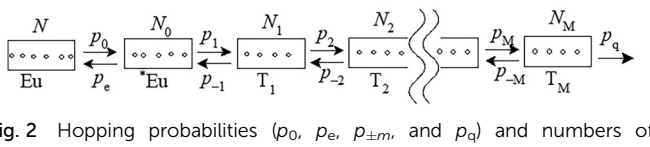

Fig. 2 Hopping probabilities (p_0, p_e, $p_{\pm m}$, and p_q) and numbers of electrons (N, N_0, and N_m) at reservoirs (Eu, *Eu, and T_m) aligned in a straight line ($m = 1 - M$). Boxes are electron reservoirs, and small circles are excited electrons involved in the PersL.

$N_0^2 = N(1 - p_0)p_0 + Np_0(1 - p_e) + Np_0(1 - p_1)$, $N_1^2 = Np_0p_1$, and $N_m^2 = 0$ (m = 2, …, M). The number of electrons N_m^n (m = 0, 1, 2, …, M) at every reservoir after many steps (n) can be obtained in similar ways, which are represented as functions of step number. By converting the step number (n) into time (t), we can predict the luminescence change by time from $p_eN_0^n$. For PersL, since the photoirradiation is ceased, p_0 alone is needed to be p_0 = 0. After the first step, the numbers of electrons at *Eu and T_1 are $N_0^1 = N_0(1 - p_e - p_1) + N_1p_{-1}$ and $N_1^1 = N_0p_1 + N_1(1 - p_{-1} - p_2) + N_2p_{-2}$, respectively. After the second step, the number of electrons at *Eu *is* determined as $N_0^2 = N_0^1(1 - p_e - p_1) + N_1^1p_{-1}$. After n steps, we can analogously obtain the number of electrons at *Eu as $N_0^n = N_0^{n-1}(1 - p_e - p_1) + N_1^{n-1}p_{-1}$. For both charging and PersL processes, we perform a curve-fitting of luminescence intensity of SAOED as a function of step number n to determine p_e, $p_{\pm m}$ (m = 1, 2, …, M), p_q and N_m (m = 0, 1, 2, …, M). Since the observation of charging and PersL processes was conducted at room temperature T_{300} = 300 K, the hopping probability can be described as $p_{\pm}^{300}$. Therefore, the probability at T can be represented as eqn (5) as a function of T,

$$p_{\pm m}^{T} = p_{\pm}^{300} \exp(-\Delta E_{\pm m}/k_B)(1/T - 1/T_{300})). \quad (5)$$

Using $p_{\pm m}^{T}$, we performed a simulation of the TL spectrum for SAOED, which contributes to the determination of $\Delta E_{\pm m}$.

3. Results

3.1. Charging and PersL

We observed luminescence changes in the charging process for SAOED$_x$ (x = 2, 4, 5, 6, 8, and 10) which had been heated at 500 K for 1 h to de-trap electrons prior to the luminescence measurement. The luminescence intensities (I) at 520 nm were recorded at time intervals of 0.5 s during the continuous photoirradiation with 370 nm light, and log(I) was plotted with grey circles against log(t) as shown in Fig. 3. As can be seen from the plots, the log(I) values in the charging process exhibit complicated curves. For SAOED$_2$, SAOED$_4$, and SAOED$_5$, each log(I) increases, reaches the maximum value log(I_{max}), and then decreases. The increase in log(I) at the early stage becomes reduced with increasing x and disappeared for SAOED$_6$, SAOED$_8$, and SAOED$_{10}$. Still, the simulation, red lines, based on 1D RWM successfully reproduces the complex decay features of the charging processes for the entire samples. The SAOED$_x$ that underwent the charging process was employed for the PersL measurement. As shown in Fig. 3, the plot of each log(I) against log(t) for PersL shows an upward convex curve, suggesting that the PersL decays non-exponentially or multi-exponentially. The times when each PersL intensity becomes I_{max}/100 are t = 470 s (x = 2), 195 s (x = 4), 505 s (x = 5), 116 s (x = 6), 82 s (x = 8), and 70 s (x = 10). Among them, the SAOED$_5$ likely shows the best performance for PersL. The red lines are simulated decay curves for the PersL and consistent with the experimental results.

Each hopping probability p_m (m = e, 1, −1, 2, −2, …, or q) between reservoirs was restricted to be the same for the charging and PersL processes in the simulation and determined through curve fitting. Listed in Table 1 are p_m values converted to the hopping probabilities per second. It is noticed that the probabilities (p_5, p_{-5}, p_6, p_{-6}, p_7, and p_{-7}) for the entire samples are almost zero, which suggests the very small contribution of reservoirs T_5 T_6, and T_7 to the PersL of SAOED$_x$. In other words, we can focus on *Eu, T_1, T_2, T_3, and T_4 to analyse the charging and PersL processes. The averaged

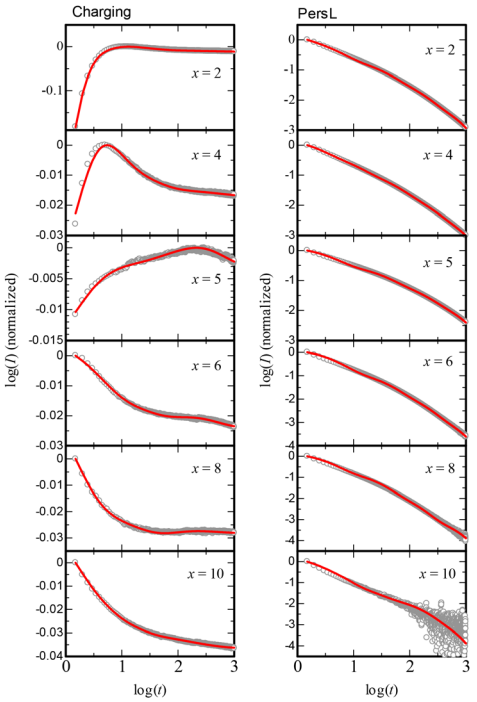

Fig. 3 (left) Changes in luminescence of SAOED$_x$ (x = 2, 4, 5, 6, 8, and 10) monitored at 520 nm in the charging process with the continuous irradiation of 370 nm at 300 K. (right) PersL of SAOED$_x$ (x = 2, 4, 5, 6, 8, and 10) monitored at 520 nm after the photoexcitation with 370 nm light for 1 min at 300 K. The relative integrated intensities of PersL for entire samples were 5.10 × 10^3 (x = 2), 2.06 × 10^3 (x = 4), 1.54 × 10^3 (x = 5), 4.30 × 10^2 (x = 6), 1.15 × 10^2 (x = 8), and 1.00 (x = 10).

Table 1 Hopping probabilities between reservoirs predicted through the simulation of charging and PersL processes for SAOED$_x$ (x = 2, 4, 5, 6, 8, and 10)

		p_1	p_2	p_3	p_4	p_5	p_6	p_7	
x	p_e	p_{-1}	p_{-2}	p_{-3}	p_{-4}	p_{-5}	p_{-6}	p_{-7}	p_q
2	0.312	0.218	0.166	0.009	0.002	0.000	0.074	0.083	0.068
		0.410	0.061	0.012	0.002	0.039	0.026	0.019	
4	0.338	0.157	0.042	0.007	0.003	0.001	0.083	0.032	0.186
		0.154	0.034	0.007	0.001	0.000	0.000	0.000	
5	0.233	0.115	0.369	0.012	0.002	0.000	0.099	0.032	0.067
		0.200	0.135	0.010	0.002	0.000	0.000	0.000	
6	0.280	0.064	0.109	0.006	0.001	0.000	0.099	0.032	0.059
		0.152	0.076	0.012	0.002	0.000	0.000	0.000	
8	0.328	0.082	0.294	0.007	0.001	0.000	0.100	0.032	0.188
		0.236	0.165	0.015	0.002	0.000	0.000	0.000	
10	0.469	0.164	0.077	0.019	0.001	0.000	0.099	0.032	0.000
		0.380	0.067	0.014	0.003	0.000	0.000	0.000	
Ave	0.330	0.116	0.178	0.010	0.001	0.001	0.096	0.032	0.111
		0.224	0.096	0.016	0.002	0.000	0.000	0.000	

hopping-probability from *Eu to T_1 (p_1) is as half as the average probability p_e, corresponding to the intrinsic relaxation probability from excited $*Eu^{2+}$ in $SAOED_x$. This result means that the 5d electron in the luminescence center easily transfers to the adjacent trap, leading to PersL for the $SAOED_x$ system. The simulation can provide the number of electrons N_m at reservoirs. Fig. S3 (ESI†) shows N_m (m = 0–6) for $SAOED_x$ (x = 2, 4, 5, 6, 8, and 10), where N_0 is normalized to unity. It is obvious that N_5 and N_6 are almost zero for the entire samples; there is no population of excited electrons. N_2, N_3, and N_4 for $SAOED_5$ are larger than those for the other samples, respectively. This result seems to relate to the best performance in PersL for $SAOED_5$.

3.2. Thermoluminescence

In Fig. 4, the thermoluminescence (TL) spectrum of each sample is plotted with grey circles from 200 to 400 K. We notice that the TL intensities of the entire samples increase from 0 at 200 K to the maximum value in the range of 250–300 K and decrease to 0 at 400 K. The peak of each spectrum would correspond to the trap depth in the corresponding sample. With increasing x, the peak temperature likely shifts to the low temperature region. It is suggested that the less the Eu^{2+} content (x) in $SAOED_x$, the deeper the trap depth. In addition, each spectral profile strongly depends on x. For example, we can see two peaks in the TL spectra of $SAOED_2$ and $SAOED_4$ but one for the others. We performed simulations of the TL spectra based on the RWM. In this simulation, the temperature dependence in hopping probability was incorporated using the following relationship:

$$p_{m,T} = p_{m,300} \exp(-(\Delta E_m/k_B)(1/T - 1/300)), \quad (6)$$

where $p_{m,300}$ (m = 1, −1, 2, −2, …, q) is the hopping probability at 300 K determined through the simulation of charging and PersL processes, k_B is Boltzmann's constant, and ΔE_m is the activation energy for hopping between reservoirs. As shown in Fig. 4, the simulated TL spectra plotted with red lines are consistent with the experimental spectra of the entire samples. Specifically, the twin peaks for $SAOED_2$ are also well reproduced through the simulation. For each sample, we can prepare a potential energy diagram for the activation states and reservoirs from the resultant ΔE_m as shown in Fig. 5, where the potential energies of them are relatively depicted with respect to that of *Eu. For the entire samples, the energies of T_1 are lower than those of *Eu, and the activation energies ΔE_1 from *Eu to T_1 are 12 kJ mol^{-1} or less. These results strongly suggest that the 5d electron in the excited state of Eu^{2+} spontaneously transfers to the next trap T_1. The ΔE_{-1} values for the backward hopping from T_1 to *Eu are 35 kJ mol^{-1} (x = 2), 34 kJ mol^{-1} (x = 4), 27 kJ mol^{-1} (x = 5), 29 kJ mol^{-1} (x = 6), 24 kJ mol^{-1} (x = 8), and 20 kJ mol^{-1} (x = 10). With an increase in the Eu^{2+} content x, the electrons at T_1 seem to become easier to move back to *Eu. This can reasonably account for the low temperature shift of peak temperature in TL when x is increased. For $SAOED_2$ and $SAOED_4$, both ΔE_2 and ΔE_{-2} are large, that is, the activation states between T_1 and T_2 are energetically high compared with the others. Most electrons are suggested to be accommodated in the relatively deep traps T_1 and/or T_2, which might be related to the twin peaks in each TL spectrum of $SAOED_2$ and $SAOED_4$. For $SAOED_5$, T_1, T_2, and T_3 sink together, and the activation energy ΔE_4 for hopping from T_3 to T_4 is remarkably large. These results suggest that the most excited electrons are populated in traps of T_1 through T_3. Although a high activation barrier of ΔE_4 is found for $SAOED_6$, the excited electrons would be mostly accommodated in T_1 because T_2 and T_3 are higher in energy than T_1. For $SAOED_8$, it is considered that the electron populations at T_1 and T_3 are larger than the others. For $SAOED_{10}$, it is characteristic that the reservoirs T_1 through T_4 act as sinks

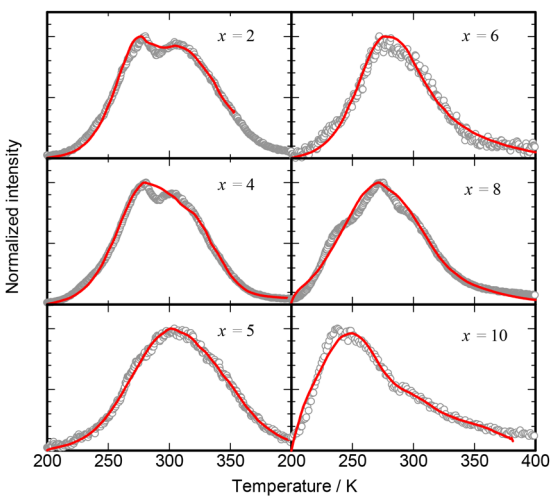

Fig. 4 TL spectra (grey circles) and their simulations (red lines) for $SAOED_x$ (x = 2, 4, 5, 6, 8, and 10). The samples were treated with the de-trapping at 500 K and the charging with 370 nm light for 10 min at 200 K. The luminescence of each sample was measured at 520 nm from 200 to 500 K with the increasing rate of 1.03 K s^{-1} after 10 min in the dark at 200 K.

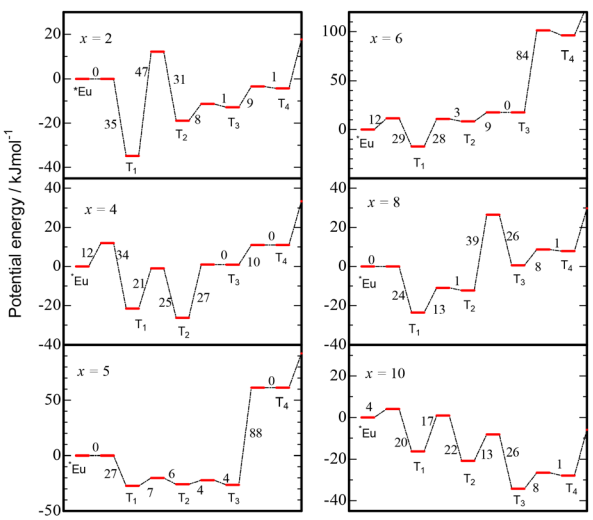

Fig. 5 Potential energy diagrams of *Eu and T_m (m = 1–4) for SAOEDx (x = 2, 4, 5, 6, 8, and 10) predicted by the simulation based on the RWM. The numbers are ΔE values in kJ mol^{-1} between the electron reservoir (*Eu or T_m) and the activation state, respectively.

compared with *Eu. This result may suggest that the excited electrons are widely distributed over T_1 through T_6.

4. Discussion

4.1. Multiple traps

X-ray crystallography revealed that there are two Sr^{2+} sites (Sr1 and Sr2) in host crystal $SrAl_2O_4$, where both Sr^{2+} sites are crystallographically nonequivalent to each other yet very similar in coordination structure.[24] These Sr^{2+} sites in the $SrAl_2O_4$:Eu^{2+} crystal can be exchanged with dopant Eu^{2+} due to their similar ionic radii of 1.21 Å (Sr^{2+}) and 1.20 Å (Eu^{2+})[25] and the same electric charges. Since the electronic configuration of excited Eu^{2+} is represented as $4f^65d^1$ involving the 5d orbital, the excited energy is sensitive to the difference in coordination geometry. Therefore, the modulation of coordination number of Eu^{2+} by O atoms by varying the SrO/Al_2O_3 ratio of host material results in the drastic change in the emission peak from 275 nm for $SrAl_{12}O_{19}$:Eu^{2+} to 467 nm for $Sr_3Al_2O_6$:Eu^{2+}.[26] $SrAl_2O_4$:Eu^{2+} emits blue and green luminescence peaking at 455 and 520 nm, respectively, which are assigned to the emission from *Eu^{2+} at Sr1 and Sr2.[26,27] The DFT calculation predicted that co-dopant Dy^{3+}, as well as Eu^{2+}, occupies the most energetically stable Sr^{2+} site.[27] This is consistent with the result of field-emission scanning electron microscopy (FE-SEM) that Eu^{2+} and Dy^{3+} are evenly distributed in the $SrAl_2O_4$ host.[28] On the other hand, another SEM measurement suggests the agglomeration of Dy^{3+} at grain boundaries in $SrAl_2O_4$.[11] Given these reports for the SAOED structure, we should consider that there are a variety of coordination structures around Eu^{2+} and Dy^{3+} for SAOED depending on its crystal structure and the contents of Eu^{2+} and Dy^{3+}. Especially, the variation in the coordination structure around Dy^{3+} will result in a variety of trap depths contributing to the multi-exponential PersL decay. Despite the complex trap system in SAOED, the simple 1D RWM is effective for the simulation of the charging and PersL processes and the TL spectra and contributes to the prediction of the traps and activation states in the SAOED crystals. The validity of the 1D trap array assumption would be rationally accounted for by the electron hopping path which can be uniquely determined when the hopping preferentially occurs between the closest traps in the crystal.

4.2. Analysis using the triple-exponential function

For $SAOED_2$, we observed the rise-and-decay curve for the change in luminescence intensity during the charging process as mentioned above. In accordance with the global system consisting of a single *Eu–trap system with a conduction band, the luminescence rise at the early stage is accounted for by the increase in the number of excited electrons in the *Eu–trap system due to the continuous photoirradiation. When a curve fitting using an equation incorporating the rise component was carried out (Fig. S4, ESI†), we needed two additional decay components to match the simulation with the experimental result. This strongly suggests that the number of excited electrons at the luminescence centre *Eu does not remain constant even after filling them up. In this simulation, we employed eqn (7),

$$I_c = I_{c1}\exp(-t/\tau_{c1}) + I_{c2}\exp(-t/\tau_{c2}) + I_{c3}\exp(-t/\tau_{c3}) + I_{c0} \quad (7)$$

where τ_{c1}, τ_{c2}, and τ_{c3} are lifetimes, I_{c2}, I_{c2}, and I_{c3} are pre-exponential factors, and I_{c0} is a constant. From the best fit, we determined τ_{c1} = 44 s, $\tau_{c2} = 5.1 \times 10^4$ s, and τ_{c3} = 1.3 s, I_{c1} = 0.025, I_{c2} = 0.26, and I_{c3} = −1.1, and I_{c0} = 0.72, as listed in Table S2 (ESI†). The electron filling process represented by the rise component is likely completed within τ_{c3} = 1.3 s in the present case. The decay components would correspond to electron transfer from the luminescence centre to traps and/or leaking electrons from the *Eu–trap system along with no luminescence such as quenching or dropping into deep traps. It might be essential that the electron transfer rate from *Eu to traps involved in PersL of $SAOED_2$ is slow. At the later stage showing the constant intensity I_{c0} = 0.72, the electron filling rate is likely balanced with the electron consuming rates due to the leaking and the luminescence emission. For PersL of $SAOED_2$, Fig. S4 (ESI†) shows that a curve fitting using eqn (8) provides the best result and affords τ_{p_1} = 5.0 s (89%), τ_{p_2} = 65 s (10%), and τ_{p_3} = 430 s (1%),

$$I_p = I_{p_1}\exp(-t/\tau_{p_1}) + I_{p_2}\exp(-t/\tau_{p_2}) + I_{p_3}\exp(-t/\tau_{p_3}). \quad (8)$$

This triple exponential function strongly suggests that there are at least three electron-trapping sites or reservoirs involving the PersL decay of $SAOED_2$. For the other samples, the simulation using eqn (7) and (8) successfully reproduced the luminescence changes in the charging and PersL as shown in Fig. S4 (ESI†). The parameters determined by the simulation are listed in Table S2 (ESI†). The resultant τ_{p_1}, τ_{p_2}, and τ_{p_3} for PersL of each sample are roughly the same: τ_{p_1} = 3–7 s (*ca.* 90%), τ_{p_2} = 27–71 s (*ca.* 10%), and τ_{p_3} = 170–450 s (*ca.* 1%). No remarkable change in lifetimes is observed. On the other hand, for the charging process, although the result for $SAOED_4$ is similar to that for $SAOED_2$, the others are different. For $SAOED_5$, two rise components, I_{c2} = −0.025 (τ_{c2} = 3.0 s) and I_{c3} = −0.0083 (τ_{c3} = 70 s), are needed to fit the experimental luminescence change. For $SAOED_6$ and $SAOED_8$, the luminescence change in the charging process can be reproduced with two decay components, since the third component is negligibly small. For $SAOED_{10}$, three decay components are needed to reproduce the luminescence change. Although we can estimate lifetimes for the charging and PersL processes based on eqn (7) and (8), it seems hard to clarify the role of traps in the luminescence behaviours in the entire $SAOED_x$, even when we take multi-traps in a SAOED crystal into account for the PersL decay and the charging process. In contrast, it is significant that the stochastic analysis using the RWM can predict the energy diagram of *Eu and traps, the electron hopping probabilities between traps, and the electron distribution in traps for the entire samples.

4.3. Trap depth from TL spectra

According to the literature,[29–31] we can determine the trap depth (E) for each $SAOED_x$ from the corresponding TL spectrum, assuming the single luminescence centre-single trap

Table 2 Trap depths (E_1 and E_2 in kJ mol^{-1}) for SAOED$_x$ (x = 2, 4, 5, 6, 8, and 10) evaluated from the TL spectra, obtained from eqn (3) and (4), respectively. ΔE_d values in kJ mol^{-1} are determined from the potential energies of deepest reservoirs for SAOED$_x$, respectively, with respect to that for *Eu

x	2	4	5	6	8	10
E_1 (kJ mol^{-1})	53.3	41.3	32.6	38.6	73.5	84.4
E_2 (kJ mol^{-1})	63.5	40.5	68.5	64.4	93.6	99.8
ΔE_d (kJ mol^{-1})	35	26	27	17	24	34

system. To do so, we created a plot of $\ln(T^2/\beta)$ *vs.* $1/k_BT$ in accordance with Hoogenstraaten's equation:[29]

$$\ln\left(\frac{T^2}{\beta}\right) = \frac{E_1}{k_B T} + \ln\left(\frac{E_1}{k_B s}\right) \quad (9)$$

where T is the peak temperature resulting from a TL spectrum, k_B is Boltzmann's constant, β is the heating rate, and s is the oscillating factor. The slope of the plot provides a trap depth E_1 for each sample, which is listed in Table 2. Alternatively, we can also determine the trap depth from eqn (10) derived from the fact that the change in β brings the shift of the peak temperature of the TL spectrum:[30,31]

$$T_2 = T_1\left(\frac{\beta_2}{\beta_1}\right)^{k_B T_1/E_2} \quad (10)$$

The trap depths (E_2) determined from this equation are listed in Table 2. The resultant E_1 and E_2 are in the range of 30–100 kJ mol^{-1}, which are consistent with the values reported by other researchers.[22] However, it seems that there is no relationship between the trap depth and the Eu^{2+} content x in SAOED$_x$. Especially, the deepest E_1 and E_2 are obtained from both methods for SAOED$_{10}$, which is inconsistent with the physical intuition that the lower the peak temperature in the TL spectrum, the shallower the trap depth. Table 2 lists energy gaps ΔE_d between *Eu and the deepest trap in SAOED$_x$ obtained through the analyses for TL spectra using the RWM. ΔE_d, the largest being 35 kJ mol^{-1} for SAOED$_2$ among them, decreases and increases with increasing x. For SAOED$_{10}$, ΔE_d is comparable to that for SAOED$_2$. It is interesting that this trend in ΔE_d against x is similar to that in E_1.

5. Conclusions

We employed SAOED$_x$ (x = 2, 4, 5, 6, 8, and 10) containing 10% dopants (Eu^{2+} and Dy^{3+}) in host crystal $SrAl_2O_4$ to produce a large amount of electron traps owing to Eu^{2+}, Dy^{3+}, oxygen vacancies, and defects. It should be noted that although the 1D trap array must be far apart from the actual arrangement of electron traps of Eu^{2+}, Dy^{3+}, oxygen vacancies, and defects in SAOED$_x$ crystals, the simulation based on the 1D RWM successfully reproduced the complicated luminescence changes in charging and PersL and the TL spectrum for each SAOED$_x$. The resultant energy diagram of the luminescence centre and traps for each sample is simple and helpful for understanding the PersL of SAOED$_x$ with a complicated trap system. The RWM is simple yet effective to visualize the picture that electrons migrate in the SAOED crystal with a variety of traps.

Author contributions

R. Koizumi and R. Takahashi conducted the preparation and identifications of materials, the luminescence measurements, and the simulation. S. Hattori and S. Yamada contributed to the experimental work and participated in discussions. K. Shinozaki supervised this project and wrote the manuscript.

Conflicts of interest

There are no conflicts to declare.

Data availability

The data supporting this article have been included as part of the ESI.†

References

1 T. Matsuzawa, Y. Aoki, N. Takeuchi and Y. Murayama, *J. Electrochem. Soc.*, 1993, **143**, 2670.
2 A. Bessière, J.-O. Durand and C. Noûs, *Nanophotonics*, 2021, **10**, 2999.
3 S. K. Sharma, D. Gourier, E. Teston, D. Scherman, C. Richard and B. Viana, *Opt. Mater.*, 2017, **63**, 51.
4 X. Tang, E. D. Ehler, E. Brost and D. C. Mathew, *J. Appl. Clin. Med. Phys.*, 2021, **22**, 191.
5 S. Singh, V. Tanwar, A. P. Simantilleke and D. Singh, *Nano-Struct. Nano-Objects*, 2020, **21**, 100427.
6 J. Xu and S. Tanabe, *J. Lumin.*, 2019, **205**, 581.
7 H. F. Brito, J. Hölsä, T. Laamanen, M. Lastusaari, M. Malkamäki and L. C. V. Rodrigues, *Opt. Mater. Express*, 2012, **2**, 371.
8 C. Chiatti, C. Fabiani and A. L. Pisello, *Annu. Rev. Mater. Res.*, 2021, **51**, 409.
9 K. Van den Eeckhout, P. F. Smet and D. Poelman, *Materials*, 2010, **3**, 2536.
10 R. E. Rojas-Hernandez, F. Rubio-Marcos, M. Á. Rodriguez and J. F. Fernandez, *Renewable Sustainable Energy Rev.*, 2018, **81**, 2759.
11 D. Van der Heggen, J. J. Joos, A. Feng, V. Fritz, T. Delgado, N. Gartmann, B. Walfort, D. Rytz, H. Hagemann, D. Poelman, B. Viana and P. F. Smet, *Adv. Funct. Mater.*, 2022, **32**, 2208809.
12 C. Jia, D. Gao, Z. Wang, X. Zhang, S. Yun, J. Z. Zhang and X. Wang, *Mater. Today Chem.*, 2024, **39**, 102182.
13 H. Li, R. Li and C. Chang, *Ceram. Int.*, 2021, **47**, 30156.
14 T. Delgado, N. Gartmann, B. Walfort, F. LaMattina, M. Pollnau, A. Rosspeintner, J. Afshani, J. Olchowka and H. Hagemann, *Adv. Photonics Res.*, 2022, **3**, 2100199.
15 A. J. J. Bos, N. R. J. Poolton, J. Wallinga, A. Bessière and P. Dorenbos, *Radiat. Meas.*, 2010, **45**, 343.

16 J. Botterman, J. J. Joos and P. F. Smet, *Phys. Rev. B:Condens. Matter Mater. Phys.*, 2014, **90**, 085147.
17 C. Tydtgat, K. W. Meert, D. Poelman and P. F. Smet, *Opt. Mater. Express*, 2018, **6**, 844.
18 P. Dorenbos, *J. Lumin.*, 2000, **91**, 155.
19 P. Dorenbos, *J. Lumin.*, 2003, **104**, 239.
20 K. Ikegaya, S. Yamada and K. Shinozaki, *Dalton Trans.*, 2019, **48**, 6746.
21 M. L. Chithambo, A. H. Wako and A. A. Finch, *Radiat. Meas.*, 2019, **97**, 1.
22 P. Zeng, X. Wei, M. Yin and Y. Chen, *J. Lumin.*, 2018, **199**, 400.
23 K. Van den Eeckhout, A. J. J. Bos, D. Poelman and P. F. Smet, *Phys. Rev. B:Condens. Matter Mater. Phys.*, 2013, **87**, 045126.
24 V. Vitola, D. Millers, I. Bite, K. Smits and A. Spustaka, *Mater. Sci. Tech. Ser.*, 2019, **35**, 1.
25 F. Clabau, X. Rocquefelte, S. Jobic, P. Deniard, M.-H. Whangbo, A. Garcia and T. Le Mercier, *Chem. Mater.*, 2005, **19**, 3904.
26 D. Dutczak, T. Jüstel, C. Ronda and A. Meijerink, *Phys. Chem. Chem. Phys.*, 2015, **19**, 15236.
27 K. Hoang, *Phys. Rev. Appl.*, 2023, **19**, 024060.
28 M. Zheng, X. Li, Y. Bai, S. Tang, P. Li and Q. Zhu, *Coatings*, 2023, **13**, 1050.
29 W. Hoogenstraaten, *Philips Res. Rep.*, 1958, **13**, 515.
30 R. Chen, J. L. Lawless and V. Pagonis, *Radiat. Meas.*, 2022, **150**, 106692.
31 M. Maghrabi, *J. Lumin.*, 2018, **198**, 54.